

This is to certify that the thesis entitled

DESIGN OF EXPERIMENTS FOR THERMOELECTRIC MATERIALS

presented by

KIMBERLY A. SARBO

has been accepted towards fulfillment of the requirements for the

M.S. degree in Mechanical Engineering

Hayld 1. Albuh

Major Professor's Signature

8/23/06

Date

MSU is an Affirmative Action/Equal Opportunity Institution

LIBRARY Michigan State University

PLACE IN RETURN BOX to remove this checkout from your record. TO AVOID FINES return on or before date due. MAY BE RECALLED with earlier due date if requested.

DATE DUE	DATE DUE	DATE DUE		
	-			
		<u> </u>		

2/05 p:/CIRC/DateDue.indd-p.1

DESIGN OF EXPERIMENTS FOR THERMOELECTRIC MATERIALS

By

Kimberly A. Sarbo

A THESIS

Submitted to
Michigan State University
in partial fulfillment of the requirements
for the degree of

MASTER OF SCIENCE

Department of Mechanical Engineering

2006

ABSTRACT

DESIGN OF EXPERIMENTS FOR THERMOELECTRIC MATERIALS

By

Kimberly A. Sarbo

Direct conversion of heat energy to electricity has many applications. One application of this technology is utilizing the heat from a nuclear reactor in a submarine to generate electricity. Thermoelectric modules can also be used to convert the wasted heat energy from an internal combustion engine directly to electric machines in a hybrid vehicle. The goal of the following research is to use statistical methods to find the optimal thermoelectric material in order to maximize the efficiency of the conversion of rejected heat energy to useful work.

When a temperature gradient is applied across a thermoelectric module, an electric current is produced. However, in order to make these modules practical, more efficient materials must be developed. This presentation outlines how a D-Optimal, four-component mixture experiment based on a silver, lead, antimony, and tellurium system was used for this optimization.

For the ranges tested, resistance, ZT, and electrical conductivity were maximized when lead levels were high and tellurium levels were low. However, an inverse relationship appeared between silver and antimony levels. ZT increased when silver was higher and antimony was lower; the opposite trends appeared in the electrical conductivity and resistance data.

Acknowledgements

I would like to thank the many people that helped me over the course of this research project. First, I would like to thank Dr. Harold Schock for giving me the opportunity to work at the Automotive Research Experiment Station. Secondly, I owe a great deal to Dr. John Cornell and Dr. Wendell Smith for supplying me with an endless amount of statistical knowledge and expertise. Both of these men provided consulting on this project without compensation; their only goal was to help a student solve a difficult problem. I must also recognize the help of Dr. Mercouri Kanatzidis and his research team. In addition, I appreciate the helpfulness of Dr. Tim Hogan and his research group, including Adam Downey and Jarrod Short. I would also like to thank Ed Timm for helping on this project, including making all the thermoelectric material. Thanks to Dr. Giles Brereton and Dr. Tim Hogan for serving on my advisory committee. I must also recognize and thank Pat Schock and Mulyanto Poort for editing this thesis and assisting with various aspects of this work. I would like to thank all those at the Automotive Research Experiment Station including Jia Ma, Melissa Jopke, Tom Stueken, Andreas Panayi, Boon Keat Chui, Josh Bedford, and Mayank Mittal. I would also like express my gratitude for the support of Andy Fedewa throughout this entire endeavor. Finally, I would like to thank my parents, Rod and Jeanette Sarbo, for their support and for making my collegiate experience possible.

TABLE OF CONTENTS

List of Tables	vi
List of Figures	vi
List of Symbols and Abbreviations	х
CHAPTER 1	
Introduction	
1.1 Motivation	
1.1.1 Motivation for Thermoelectric Materia	als1
1.1.2 Motivation for Design of Experiments	2
1.2 Previous Work	
1.3 Introduction to Thermoelectric Materials	4
1.4 Introduction to Design of Experiments	
CHAPTER 2	
Experimental Equipment and Procedure	16
2.1 Mixture Selection and Experimental Setup	
2.1.1 Design-Expert® Software	
2.2 Material Preparation	
2.2.1 Vacuum Sealing Line and Pump	
2.2.2 Furnace and Temperature Control Sys	
2.2.3 Leematic 2000 Surface Grinder and S	
2.3 Data Collection	
2.3.1 Four-Point Probe	
2.3.2 ZT Machine	
CHAPTER 3	
Results and Discussion	30
3.1 Resistance	
3.2 ZT	
3.3 Electrical Conductivity	
CHAPTER 4	
Conclusions	47
CHAPTER 5	
Recommendations	50
Appendices	51
Appendix A Additional Plot	50
A MAGNITURE A TUTO CONTROL OF THE PROPERTY OF	

Appendix B ZT and Electrical Conductivity	Data53
References	57

List of Tables

Table 1.	The number of terms for some Scheffé polynomials for q components	13
Table 2.	Molar composition of design points.	18
Table 3.	Mass composition of design points	19
Table 4.	ANOVA for quadratic model of transformed resistance response	35
Table 5.	R ² values and adequate precision for the transformed resistance response fi	
Table 6.	ANOVA for quadratic model of ln(ZT) response.	39
Table 7.	R ² values and adequate precision for ln(ZT) response fit	39
Table 8.	ANOVA for quadratic model of electrical conductivity data	43
Table 9.	R ² values and adequate precision for electrical conductivity response	43
Table 10.	Optimized component levels for tested properties.	49

List of Figures

Figure 1.	Temperature and voltage gradients across a thermoelectric leg	5
Figure 2.	Example resistivity measurement on a thermoelectric leg.	6
Figure 3.	A thermoelectric couple	7
Figure 4.	Module configuration exploded view (left) and assembled (right)	7
Figure 5.	A proposed thermoelectric generator design consisting of six modules	8
Figure 6.	Comparison of factorial (2 factors, 2 levels) and mixture designs for 2 components.	9
Figure 7.	Examples of two-, three-, and four-component mixture spaces, respectively	.10
Figure 8.	A Constrained-region, four-component mixture space.	11
Figure 9.	Mixture space with axes and point location for $(A, B, C) = (1/6, 1/2, 1/3)$	12
Figure 10.	Sample 2-dimensional contour and 3-dimensional surface plots	15
Figure 11.	Vacuum sealing system.	20
Figure 12.	Furnace closed (left) and open (right).	21
Figure 13.	Computer and ATS Controller.	21
Figure 14.	Furnace temperature as a function of time.	22
Figure 15.	Leematic 2000 Surface Grinder and Slicer.	23
Figure 16.	Coin and leg orientation in a cast thermoelectric ingot	24
Figure 17.	Four-point probe.	25
Figure 18.	Electrical diagram of the ZT Machine.	26
Figure 19.	The ZT Machine (pictured without the outer vacuum chamber)	27
Figure 20.	A close-up of mounted legs on the ZT Machine.	27
Figure 21.	Example plot of resistance vs. frequency for a thermoelectric leg	28

Figure 22.	Correlation plot between tellurium and lead31
Figure 23.	Resistance data plotted by design point
Figure 24.	Internally studentized residuals vs. predicted resistance without inverse square root transformation
Figure 25.	Internally studentized residuals vs. predicted resistance with inverse square root transformation
Figure 26.	Predicted vs. Actual plot for resistance without transformation or ignored points
Figure 27.	Predicted vs. Actual plot for resistance with point 14 ignored and the inverse square root transformation applied34
Figure 28.	Contour plot of resistance at tellurium equal to 37.945 grams36
Figure 29.	Contour plot of resistance at tellurium equal to 39.42 grams36
Figure 30.	Contour plot of resistance at tellurium equal to 40.894 grams37
Figure 32.	Contour plot of ZT at tellurium equal to 37.945 grams
Figure 33.	Contour plot of ZT at tellurium equal to 39.42 grams40
Figure 34.	Contour plot of ZT at tellurium equal to 40.894 grams
Figure 35.	Electrical conductivity data plotted by design point42
Figure 36.	Contour plot of electrical conductivity at tellurium equal to 37.945 grams44
Figure 37.	Contour plot of electrical conductivity at tellurium equal to 39.42 grams44
Figure 38.	Contour plot of electrical conductivity at tellurium equal to 40.894 grams45
Figure 39.	Contour plot of electrical conductivity at tellurium equal to 40.894 grams where all points were included in the analysis
Figure 40.	Three-dimensional view of resistance response surface at tellurium equal to 39.42 grams
Figure 41.	Three-dimensional view of ZT response surface at tellurium equal to 39.42 grams

Figure 42.	Three-dimensional view of electrical conductivity response surface at tellurium equal to 39.42 grams.	48
Figure 43.	ZT vs. Electrical Conductivity for all design points.	52
Figure 44.	Data collected using ZT Machine (part 1).	53
Figure 45.	Data collected using ZT Machine (part 2).	54
Figure 46.	Data collected using ZT Machine (part 3).	55
Figure 47.	Data collected using ZT Machine (part 4).	56

Images in this thesis are presented in color.

List of Symbols and Abbreviations

A cross-sectional area

AC alternating current

cm centimeters

DC direct current

g grams

I current

l length

K Kelvin

m mass

mol moles

q number of mixture components

R resistance

s spacing

S Siemens

T temperature

u atomic mass (grams)

α Seebeck coefficient

ρ electrical resistivity

σ electrical conductivity

 λ thermal conductivity

CHAPTER 1

Introduction

1.1 Motivation

1.1.1 Motivation for Thermoelectric Materials

This thesis is based on the thermoelectric effect discovered by Seebeck. Put simply, the system in this project provides a temperature gradient from which an electric current will be created and used for other applications. One application of this technology is utilizing the heat from a nuclear reactor in a submarine to generate electricity. Thermoelectric modules can also be used to convert the wasted heat energy from an internal combustion engine directly to electric machines in a hybrid vehicle. It has been shown that from the energy in a given gallon of fuel, as much as 35% of the energy is expelled as exhaust gases, and as much as 25% of the energy is released from other various heat transfer losses. Thus, an engine is only using a fraction of the energy provided by the fuel to propel the vehicle. The goal of the following research is to use statistical methods to find the optimal thermoelectric material in order to utilize as much as possible of the unused heat energy as possible.

Thermoelectric devices have many advantageous qualities over alternative devices, such as:

- Comparatively lightweight, and small in size
- Heat pumping process is reversible
- There are no moving parts
- Very reliable (over 100,000 hours of operation)
- Very fine temperature control with the correct electronic system

- No consumables
- Generators can take on many different configurations for different applications
- Thermoelectric devices can be designed to be small without a change in efficiency

The main disadvantage of thermoelectric systems is the low efficiency. The average generators on the market have a conversion efficiency of approximately 5%. However, even a small increase in efficiency for an engine system would result in increased engine life due to a decrease in engine stress.

1.1.2 Motivation for Design of Experiments

Design of experiments provides an organized, statistically sound method of determining and executing experiments. There are many varieties of experiments, all with different applications, strengths, and weaknesses. The main motives for using design of experiments are the following:

- Designed experiments are efficient and systematic
- The response can be analyzed with respect to one or more factors
- Error, variance, and other statistical parameters can be interpreted

1.2 Previous Work

The experiments outlined in this paper were chosen based on the Ag-Pb-Sb-Te system (or 'LAST system,' standing for Lead-Antimony-Silver-Tellurium), as published by Hsu, et al. [5]. The samples AgPb₁₈SbTe₂₀ and AgPb₁₀SbTe₁₂ were reported to have high figures-of-merit. Although the results have been repeated within 20% by other research groups [22], replication of the high ZT materials has been challenging, possibly

caused by the strong stoichiometric variations in the materials under the initial fabrication techniques [6]. It is believed that a sweet spot exists in this system that may deviate slightly from the above stoichiometries due to stratification of the components. It has also been reported in the literature that LAST samples, when exposed to air, can react with oxygen thus causing compositions different to those originally formulated [22].

Kosuga et al. [8] also published data on the LAST system and reached a maximum ZT of 0.33 at 673 K for composition Ag_{0.7}Pb₁₈SbTe₂₀. The compositions AgPb₁₈SbTe₂₀, Ag_{0.9}Pb₁₈SbTe₂₀ and Ag_{0.7}Pb₁₈SbTe₂₀ exhibited the highest ZT at the lowest level of silver tested, though the method of preparation differs greatly from that outlined in this text. The results from the following mixture experiment suggest that higher levels of silver are needed relative to the ranges tested, though the highest level of silver tested for the mixture experiment is still lower than the lowest level tested by Kosuga et al. The results from the above papers, combined with subsequent experiments using the LAST system, were used to determine the component ranges for the following mixture experiment.

The motivation behind using a mixture experiment for the analysis of the LAST system is supported by several sources. Most notably, the article "Designing Mixture Experiments" by Agreda and Agreda [1] states, "experiments involving mole or mass fractions lend themselves naturally to the mixture design approach, as the mass or mole fractions add to 1 by definition." In addition, authors Cornell [2] and Smith [14], who have published on the subject of mixture experiments, provided consulting on this project in addition to the many examples in their respective publications.

1.3 Introduction to Thermoelectric Materials

The technology behind thermoelectric materials is based on the Seebeck effect. In the 19th century, Seebeck found that a metal bar with a temperature gradient across it would also have a voltage across the bar. Seebeck also found that a compass needle would be deflected when it was placed near a closed circuit of two different conductors when one of the junctions in the circuit was heated. This was due to the fact that a current flowed through the circuit, thus causing a magnetic field in the vicinity of the circuit. Unfortunately, Seebeck incorrectly reasoned that the magnetic field was responsible for the effect, and pursued this line of reasoning, rather than using his findings to make thermocouples, and thus using the temperature difference to create electricity. However, Seebeck experimented with many different materials, some of which are now classified as semiconductors [7].

The inverse of Seebeck's finding was discovered by Peltier about 13 years later. Peltier found that a temperature gradient was created when an electric current was supplied to a closed circuit composed of two different conductors. Peltier never compared his findings to those of Seebeck. It was not until 1838 that Lenz explained the Seebeck and Peltier effects. He showed that heat is transferred in a certain direction depending on the direction of the current flow in a circuit composed of two conductors [11].

The efficiency of thermoelectric materials is related to the parameter known as the figure-of-merit, Z, in equation (1.1).

$$Z = \frac{\alpha^2}{\lambda \rho} = \frac{\alpha^2 \sigma}{\lambda} \tag{1.1}$$

The unit of Z is 1/K. Since Z varies with temperature, a nondimensional figure of merit, ZT, is often used. The Seebeck coefficient, α , is a measure of the change in voltage over the change in temperature across a thermoelectric leg, as seen in Figure 1 and equation (1.2) below.

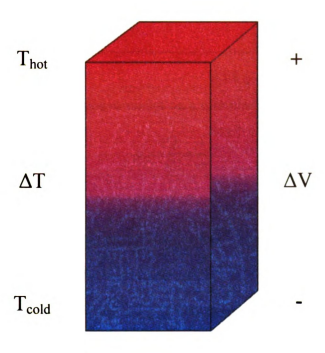


Figure 1. Temperature and voltage gradients across a thermoelectric leg.

$$\alpha = \frac{dV}{dT} \tag{1.2}$$

Thermal conductivity, λ , depends weakly on the carrier concentration of the thermoelectric material. Resistivity, ρ , is measured as seen in Figure 2, and is the inverse of electrical conductivity, σ .

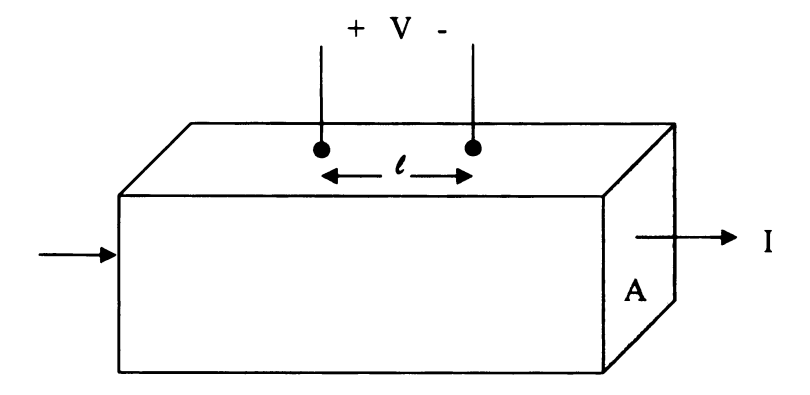


Figure 2. Example resistivity measurement on a thermoelectric leg.

$$\rho = \frac{VA}{Il} = \frac{1}{\sigma} \tag{1.3}$$

A thermoelectric module is composed of positively and negatively doped legs, hot-side material, cold-side material, and the necessary electrical wiring. The device is constructed by connecting the thermoelectric legs thermally in parallel and electrically in series. This configuration allows for the best temperature gradient across the system while providing for proper current flow. Figure 3 shows a "couple," a unit consisting of P- and N-type material connected by a conductive material, such as copper, to provide the electrical connection.

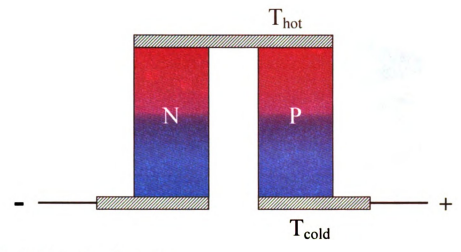


Figure 3. A thermoelectric couple.

Many of these couples are connected and sandwiched between thermally conductive plates to make modules similar to the one in Figure 4.



Figure 4. Module configuration exploded view (left) and assembled (right).

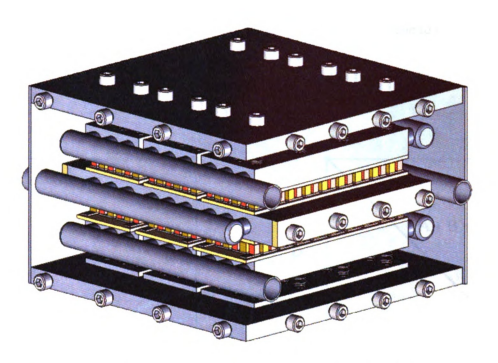


Figure 5. A proposed thermoelectric generator design consisting of six modules.

1.4 Introduction to Design of Experiments

There are many kinds of experimental designs including, but not limited to, factorial, fractional factorial, nested, and response surface designs. The simplest type of design is full factorial. This design consists of completing experiments for every combination of factors. For instance, two factors being investigated at two levels would result in 4 experimental runs. This method cannot be used for mixture experiments because factorial designs do not take proportions of components into account. Using a factorial design for a mixture experiment would result in unnecessary, repeated tests. The figure below demonstrates the difference between factorial and mixture spaces. Experimental runs are placed at the points of the factorial space, whereas runs, or design points, are placed along the constraint line in the mixture space. Response surface designs can be thought of as a hybrid of factorial and mixture designs. They can be organized similarly to designs in the factorial family, a response surface is generated

similar to those of mixture experiments, but the response does not depend on the ratios of the components.

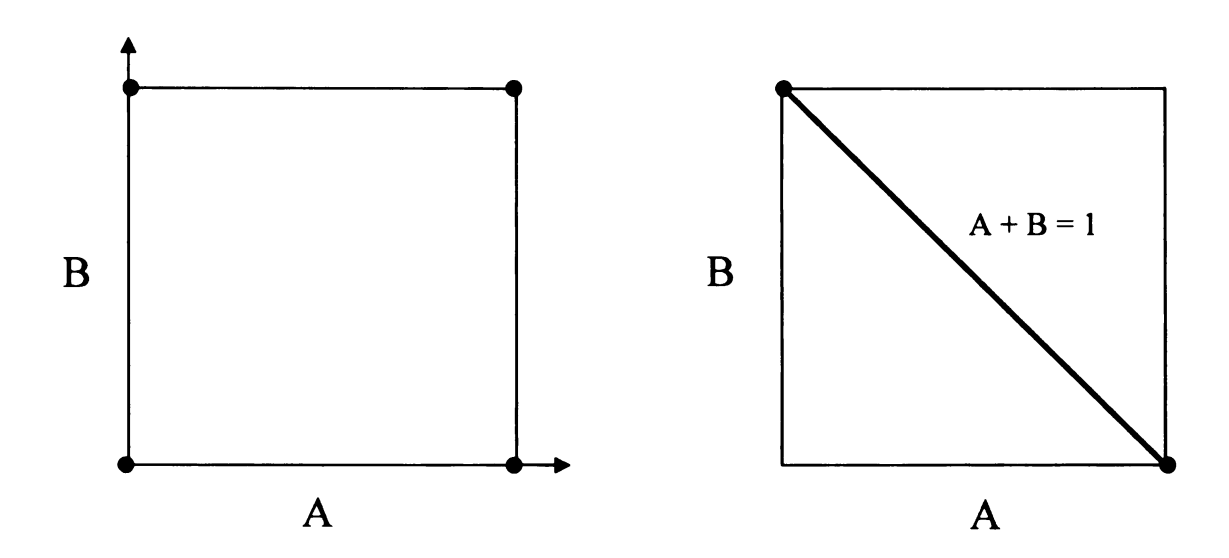


Figure 6. Comparison of factorial (2 factors, 2 levels) and mixture designs for 2 components.

The statistical analyses in this text are based on a mixture design, which is under the category of response surface designs. A D-Optimal mixture design was chosen since the design space was complex and component ranges varied in size. A D-Optimal design is also useful for reducing the error of the model coefficients. What differentiates mixtures from other designs is the constraint below, which applies for q components.

$$\sum_{i=1}^{q} x_i = 1 \tag{1.4}$$

This constraint defines the boundaries of the mixture space. Examples of simplexes for two-, three-, and four-component mixtures are shown in Figure 7, where a two-component mixture is a line, a three-component mixture is a plane, and a four-component mixture is a tetrahedron.

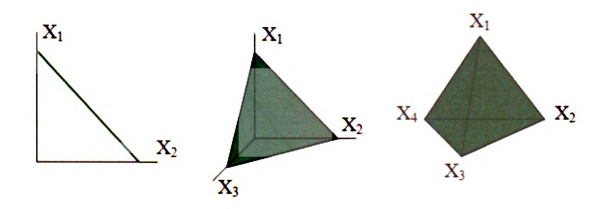


Figure 7. Examples of two-, three-, and four-component mixture spaces, respectively.

In order to accommodate the four-component, three-dimensional space response surface plot, triangular slices are plotted along one axis as seen in Figure 8. The vertices of the largest tetrahedron represent pure blends, or the design points where only one component is present. The smaller tetrahedron represents a constrained mixture space, where only certain component ranges are being investigated.

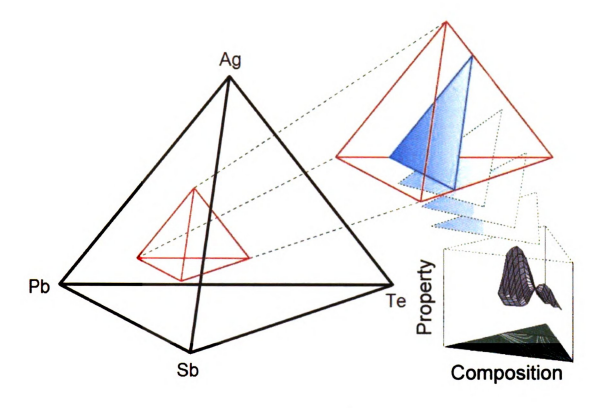


Figure 8. A Constrained-region, four-component mixture space.

Each triangular slice has three axes that extend from each vertex and bisect the opposing side, where the maximums for each component are located at the vertices. Areas outside the constraints are shaded gray. Points in the design space are located by drawing a perpendicular line across each axis at each component level. An example of locating point (A, B, C) = (1/6, 1/2, 1/3) is shown below.

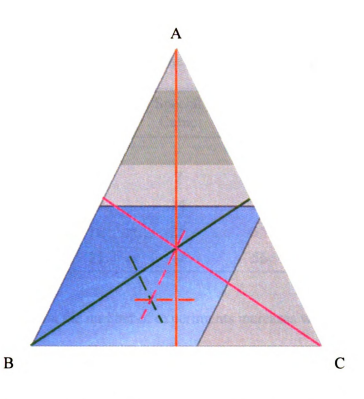


Figure 9. Mixture space with axes and point location for (A, B, C) = (1/6, 1/2, 1/3).

Design points are chosen based on the number of components and the type of curve fit needed, based on subject matter knowledge and preliminary experiments.

Examples of mixture polynomials (or curve fits) are linear, quadratic, special cubic, cubic, special quadratic, and quadratic. Table 1 shows the number of terms needed for q components for Scheffé polynomials, the standard polynomials used for most mixture experiments [12] [2] [14].

Table 1. The number of terms for some Scheffé polynomials for q components.

q	Linear	Quadratic	Special Cubic	Cubic	Special Quartic	Quartic
2	2	3	-	4	-	5
3	3	6	7	10	9	15
4	4	10	14	20	22	35
5	5	15	25	35	45	70
6	6	21	41	56	81	126

Table 1 demonstrates how the number of experiments increases with the number of components and the complexity of the contours of the response surface. A linear curve fit only requires design points at the vertices, or each of the pure blends. The quadratic model adds mixtures of two blends, or points along the edges of the design space, and so on for higher level polynomials.

In addition to the points in Table 1, design points are needed to test for lack of fit and pure error. These points are used in the statistical analysis in order to determine the correct response surface and how well the response surface fits the collected data.

Once data are collected at locations within the design space, a polynomial is used to fit a response surface. The most common polynomials used are linear, quadratic, special cubic, and cubic Scheffé polynomials. For a four-component mixture composed of A, B, C, and D, the equations for the predicted response, \hat{y} , are shown for linear (1.5), quadratic (1.6), and special cubic (1.7) curve fits, where the c_i 's represent the regression coefficients.

$$\hat{y} = c_1 A + c_2 B + c_3 C + c_4 D \tag{1.5}$$

$$\hat{y} = c_1 A + c_2 B + c_3 C + c_4 D + c_5 A B + \dots + c_{10} C D$$
 (1.6)

$$\hat{y} = c_1 A + c_2 B + c_3 C + c_4 D + c_5 A B + \dots + c_{10} C D + c_{11} A B C + \dots + c_{14} B C D$$
 (1.7)

The linear Scheffé model coefficients are estimates of the response at each of the vertices. A quadratic model can be thought of as an augmentation of the linear model, where combinations of components are being investigated. A similar augmentation is noted in the special cubic model. The effect of a component, or a combination of components, is only seen in the slope of the corresponding response surface.

A statistical software package is used to fit all predicted responses as well as the corresponding p-values for each response. P-values determine the significance of a model, or a term in a model. Graphically, a p-value for this analysis is the area under the F-curve, to the right of the calculated F-value. For most statistical applications, a model or term with a p-value of 0.05 or below is considered statistically significant. Models and terms with p-values above 0.10 are considered statistically insignificant. Lack of fit tests and model summary statistics are used to determine the model that best represents the collected data. Once the best model is chosen, an analysis of variance (ANOVA) is completed for the selected model and other statistical measures are calculated. After the statistical analysis is complete, the response surfaces are plotted in 2-dimensional contour views or 3-dimensional surface views similar to those below.

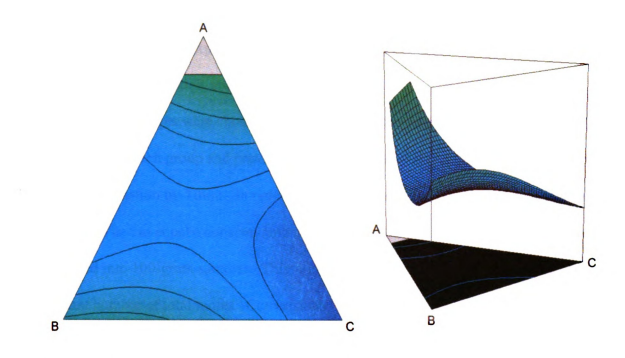


Figure 10. Sample 2-dimensional contour and 3-dimensional surface plots.

CHAPTER 2

Experimental Equipment and Procedure

2.1 Mixture Selection and Experimental Setup

Sample ranges were chosen based on the previous experiments made by the Kanatzidis research group and previous mixtures prepared at the Automotive Research Experiment Station by Timm. In order to satisfy the mixture experiment constraint that all samples had to equal a constant amount (Equation 1.1), all chemical compounds were converted into 100-gram samples. This was done since the samples did not add to a constant number of total moles. Conversions were made by choosing a reference component, silver in this case, and scaling the number of grams for all components as seen in Equations (2.1) through (2.4).

$$m_{Ag} = \left(\frac{m}{u * mol}\right)_{Ag} * mol_{Ag} * u_{Ag} = m_{Ag} * \left(\frac{u}{u}\right)_{Ag} * \left(\frac{mol}{mol}\right)_{Ag}$$
(2.1)

$$m_{Pb} = \left(\frac{m}{u * mol}\right)_{Ag} * mol_{Pb} * u_{Pb} = m_{Ag} * \left(\frac{u_{Pb}}{u_{Ag}}\right) * \left(\frac{mol_{Pb}}{mol_{Ag}}\right)$$
(2.2)

$$m_{Sb} = \left(\frac{m}{u * mol}\right)_{Ag} * mol_{Sb} * u_{Sb} = m_{Ag} * \left(\frac{u_{Sb}}{u_{Ag}}\right) * \left(\frac{mol_{Sb}}{mol_{Ag}}\right)$$
(2.3)

$$m_{Te} = \left(\frac{m}{u * mol}\right)_{Ag} * mol_{Te} * u_{Te} = m_{Ag} * \left(\frac{u_{Te}}{u_{Ag}}\right) * \left(\frac{mol_{Te}}{mol_{Ag}}\right)$$
(2.4)

2.1.1 Design-Expert® Software

The Design-Expert[®] software, developed by Stat-Ease[®], was used to perform all statistical analyses. The design of experiments program has the ability to set up an experiment, analyze data using analysis of variance as well as other tools, and display data using a variety of methods. The program offers many experimental designs

including: factorial, fractional factorial, Taguchi, Placket-Burman, response surface, and mixture designs. However, only the mixture design was needed for the purpose of this project.

Once gram ranges are found using equations (2.1) through (2.4), high and low gram amounts are entered into Design-Expert. It is necessary to enter the type of design, a D-Optimal Mixture; the highest polynomial order that can be accommodated, special cubic; and any other adjustments that are needed, such as additional design points into the program. For the purpose of this experiment the defaults of 5 replicates and 5 check blends were used for a total of 24 experimental runs. The program then generates a list of gram amounts for each of the runs, or design points, that need to be prepared and tested. Once the experimental results are entered into the software, the statistical analysis is completed, a model is chosen by the user, and color-coded contour plots are generated in order to view the response surface. Tables 2 and 3 display the list of experimental runs in moles and grams, respectively. Replicate design points are italicized. An ingot is made for each of the design points below.

Table 2. Molar composition of design points.

Design	D. ' T.	Molar Composition			
Point	Point Type	Ag	Pb	Sb	Te
1	Vertex	0.628	18	1.005	21.254
2	Plane Centroid	0.406	18	1.433	19.970
3	Triple Blend	0.610	18	1.273	19.532
4	Vertex	0.596	18	0.955	18.739
5	Vertex	0.191	18	0.955	19.051
6	Vertex	0.201	18	1.466	21.274
7	Vertex	0.629	18	1.466	20.913
8	Triple Blend	0.480	18	1.447	20.380
9	Plane Center	0.437	18	0.972	19.728
10	Center Edge	0.195	18	0.974	20.004
11	Center Edge	0.195	18	0.974	20.004
12	Vertex	0.191	18	0.955	19.051
13	Vertex	0.628	18	1.005	21.254
14	Vertex	0.596	18	0.955	18.739
15	Plane Centroid	0.431	18	1.201	18.797
16	Vertex	0.605	18	1.410	19.008
17	Plane Centroid	0.196	18	1.256	19.993
18	Axial Check Blend	0.303	18	1.320	20.627
19	Vertex	0.198	18	0.993	20.995
20	Triple Blend	0.336	18	0.984	20.411
21	Axial Check Blend	0.296	18	1.297	19.374
22	Vertex	0.201	18	1.466	21.274
23	Plane Centroid	0.617	18	1.180	20.216
24	Vertex	0.191	18	1.394	18.785

Table 3. Mass composition of design points.

Design	Doint Time	Grams			
Point	Point Type	Ag	Pb	Sb	Te
1	Vertex	1.021	56.239	1.846	40.894
2	Plane Centroid	0.674	57.413	2.686	39.227
3	Triple Blend	1.021	57.889	2.406	38.684
4	Vertex	1.021	59.188	1.846	37.945
5	Vertex	0.327	59.225	1.846	38.602
6	Vertex	0.327	56.132	2.686	40.855
7	Vertex	1.021	56.132	2.686	40.162
8	Triple Blend	0.789	56.870	2.686	39.654
9	Plane Center	0.736	58.162	1.846	39.256
10	Center Edge	0.327	58.079	1.846	39.748
11	Center Edge	0.327	58.079	1.846	39.748
12	Vertex	0.327	59.225	1.846	38.602
13	Vertex	1.021	56.239	1.846	40.894
14	Vertex	1.021	59.188	1.846	37.945
15	Plane Centroid	0.736	59.005	2.313	37.945
16	Vertex	1.021	58.348	2.686	37.945
17	Plane Centroid	0.327	57.781	2.369	39.523
18	Axial Check Blend	0.499	56.897	2.452	40.152
19	Vertex	0.327	56.933	1.846	40.894
20	Triple Blend	0.558	57.466	1.846	40.130
21	Axial Check Blend	0.499	58.352	2.471	38.678
22	Vertex	0.327	56.132	2.686	40.855
23	Plane Centroid	1.021	57.208	2.204	39.568
24	Vertex	0.327	59.042	2.686	37.945

2.2 Material Preparation

2.2.1 Vacuum Sealing Line and Pump

A BOC Edwards pump system is used to achieve the desired vacuum in the quartz ampoule during the sealing process. The system consists of a rotary pump, diffusion

pump, electrical controller, and active gauge display. The pump system is attached to a series of glass tubes and valves to control the airflow.

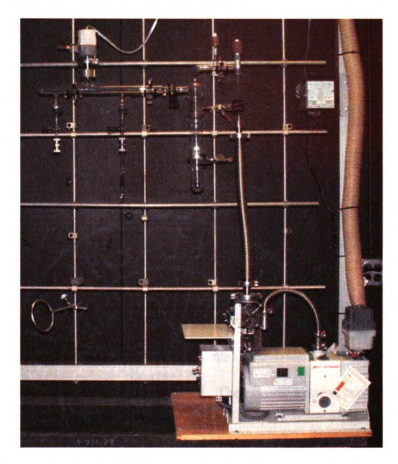


Figure 11. Vacuum sealing system.

The mixture components are weighed and put into a 22-mm diameter glass tube. A vacuum of $1x10^4$ millibar is created using the BOC Edwards pump, and the quartz tube is sealed off using a propane-oxygen torch.

2.2.2 Furnace and Temperature Control System

The furnace is a three-zone, series 3210 split-tube built by Applied Test Systems, Inc. The outer shell is stainless steel and uses Kanthal[®] A1 resistive heating elements.

The inner diameter is two inches, and the outer diameter is ten inches. The furnace is

19.25 inches in length, where 15 of those inches are heated. Each of the three five-inch-

long zones has a thermocouple port, and the furnace has one overall control thermocouple port. The furnace is rated to have a maximum temperature of 1100°C.

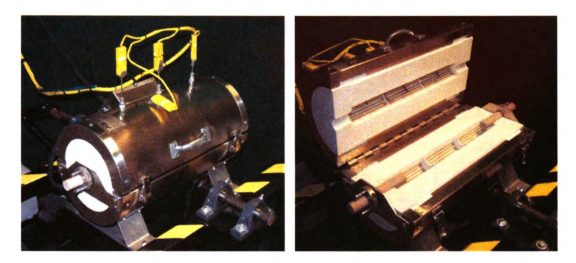


Figure 12. Furnace closed (left) and open (right).

The temperature control system, also a product of Applied Test Systems, Inc., regulates the power given to the heating elements. The system uses Barber Colman 2404 controllers to attain the specified temperature. The control system uses iTools, a software program developed by Eurotherm, Inc. which allows the user to program a heating and cooling profile for the furnace.



Figure 13. Computer and ATS Controller.

The sealed tube from the step above is placed in the ATS furnace where the mixture is heated, rocked, and cooled. The temperature is increased at 50°C/hr up to 1020°C where the liquid mixture is rocked for 8 hours. The mixture is then cooled to 850°C at 85°C/hr, then to 750°C at 5°C/hr, and finally, from 750°C to 50°C at 30°C/hr as seen in Figure 14.

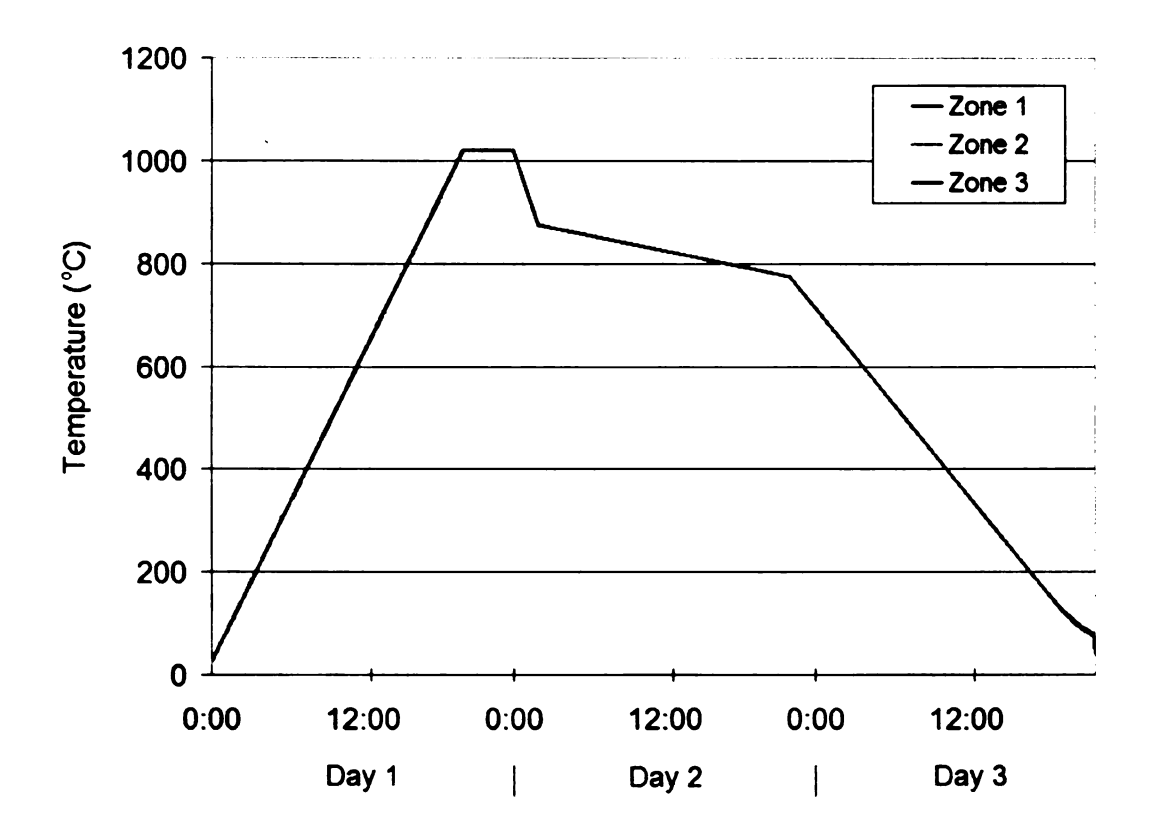


Figure 14. Furnace temperature as a function of time.

2.2.3 Leematic 2000 Surface Grinder and Slicer

The Leematic surface grinder/slicer from K.O. Lee Company utilizes a high-speed abrasive disk for making precision cuts. For this application, a diamond cutting wheel is rotated at 5000 rpm to cut the thermoelectric material. The process is controlled via a computer which actuates the three axis traverse. This allows the entire process to be automated. Multiple cutting passes are made at 5 cm/sec, each at a slightly greater depth

than the previous. Such a high-speed cutting system makes it possible to make highly accurate cuts on the relatively brittle thermoelectric materials.



Figure 15. Leematic 2000 Surface Grinder and Slicer.

After the ingots have been cooled, they are glued onto an aluminum bar for cutting. Each ingot is sliced into four coins 7 mm thick. Each coin is then individually sliced into seven 5 mm by 5 mm by 7 mm legs (Figure 16). Legs are labeled, and position within the ingot is noted for future studies.

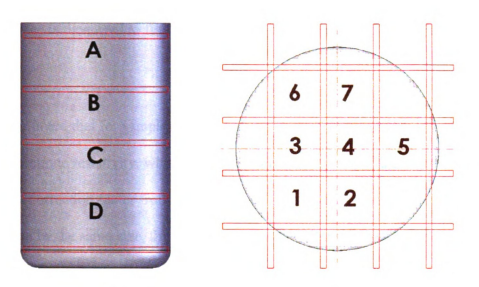


Figure 16. Coin and leg orientation in a cast thermoelectric ingot.

2.3 Data Collection

2.3.1 Four-Point Probe

Each leg was first screened using the four-point probe. Intact legs were tested on each of the four longer sides, unless a side was too damaged due to holes or cracks in the material. The probes are rested on the material for a nearly-immediate resistance reading. Holes and other imperfections can cause severe fluctuations in the resistance measurement, so some measurements were averaged or ignored, depending on the disparity between measurements. The variability between resistances of legs was a function of ingot composition or position of the leg within the ingot.

A known direct current is passed through the outer probes using a Keithley 2400 sourcemeter, and a voltage drop is measured between the inner two probes using a Keithley 2182 nanovoltmeter. Ohm's law can be used to calculate the resistance, R, of the sample (2.5).

$$R = \frac{V}{I} \tag{2.5}$$

The resistance is then used to find the resistivity, ρ , of the material using Equation (2.6).

$$\rho = \frac{RA}{l} = \frac{1}{\sigma} \tag{2.6}$$

It should be noted that for samples of finite size, a correction factor should be used to obtain an accurate resistivity, where the dimensions of the sample are used to find the appropriate correction factor from a chart. However, since all thermoelectric legs were fabricated to be the same size, the measured resistance is proportional to the corrected resistivity. Therefore, the resistance given by the four-point probe was used to make relative comparisons between samples.

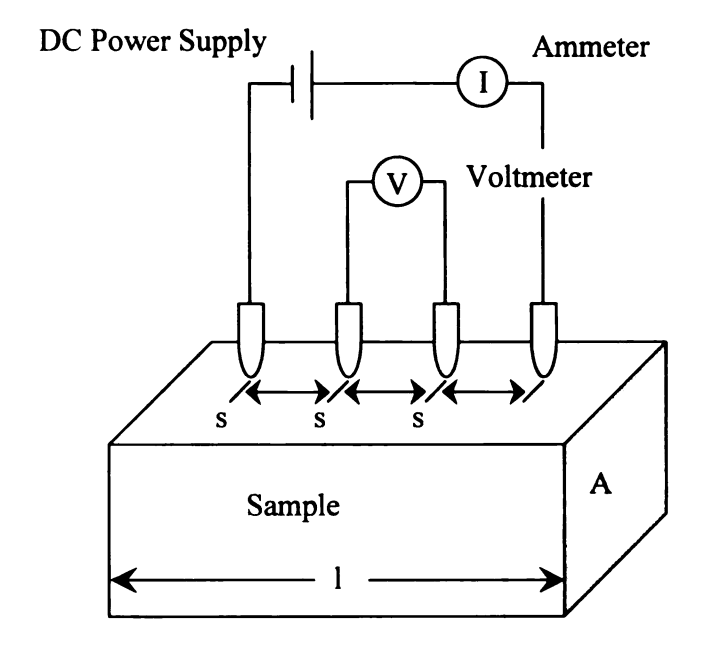


Figure 17. Four-point probe.

2.3.2 ZT Machine

The ZT Machine, developed by Adam Downey of the Hogan research group [4], is capable of measuring electrical conductivity and ZT. The apparatus is able to measure sixteen samples at a time over a period of approximately 2 ½ days. Three to ten legs

were chosen from each ingot for testing based on the lowest number of cracks and holes in the material. Flux is applied to the end of each leg; and Cerromatrix Bi 48%-Pb 28.5%-Sn 14.5%-Sb 9% solder is applied to the end of the leg and two pieces of thin copper foil. The foil and leg ends are heated to form bonds between the legs and foil pieces. The current-carrying wires are bonded to the copper foil and attached to pin and socket circuit boards for mounting to the device, so that the legs are electrically in series. A voltage difference is measured across each leg by two 0.003 inch copper wires sparkwelded to one side as seen in Figure 18. Samples are then suspended by the current-carrying wires in approximately a 10-μtorr vacuum, created using a rough pump and turbo pump, which keeps each sample in thermal isolation.

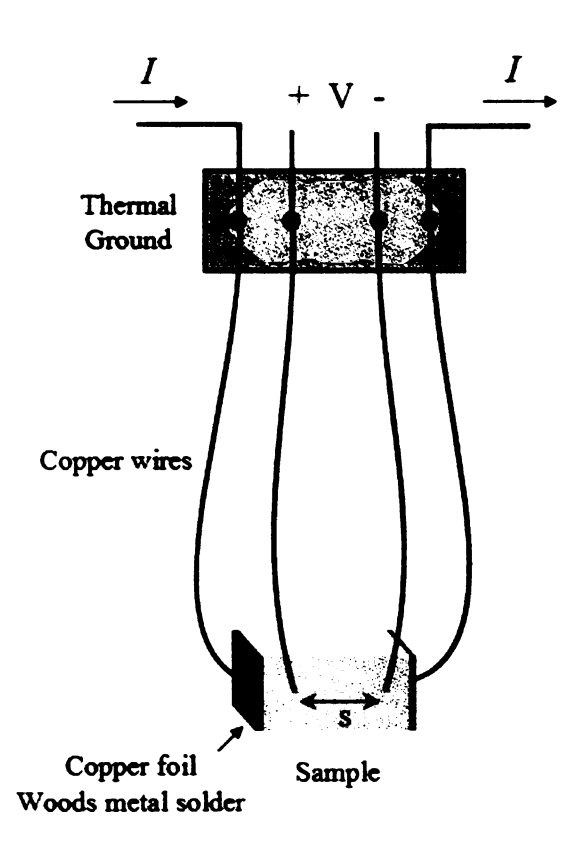


Figure 18. Electrical diagram of the ZT Machine.



Figure 19. The ZT Machine (pictured without the outer vacuum chamber).



Figure 20. A close-up of mounted legs on the ZT Machine.

Four cycles of a square wave, low frequency current of 1 mHz to 100 mHz are fed through each leg, followed by 10 cycles of high frequency current from 1 Hz to 11 Hz. The high frequency current, or alternating current, prevents the development of a temperature gradient across the thermoelectric leg. The low frequency current, or direct current, allows a temperature gradient to form. Resistance measurements are taken at both current frequencies and are used in calculating the figure of merit. An example plot of resistance vs. frequency is shown below in Figure 21. The ratio of the low frequency, or R_{DC} , measurements on the left of the plot over the high frequency, R_{AC} , measurements on the right side of the plot, minus 1, is used to determine ZT.

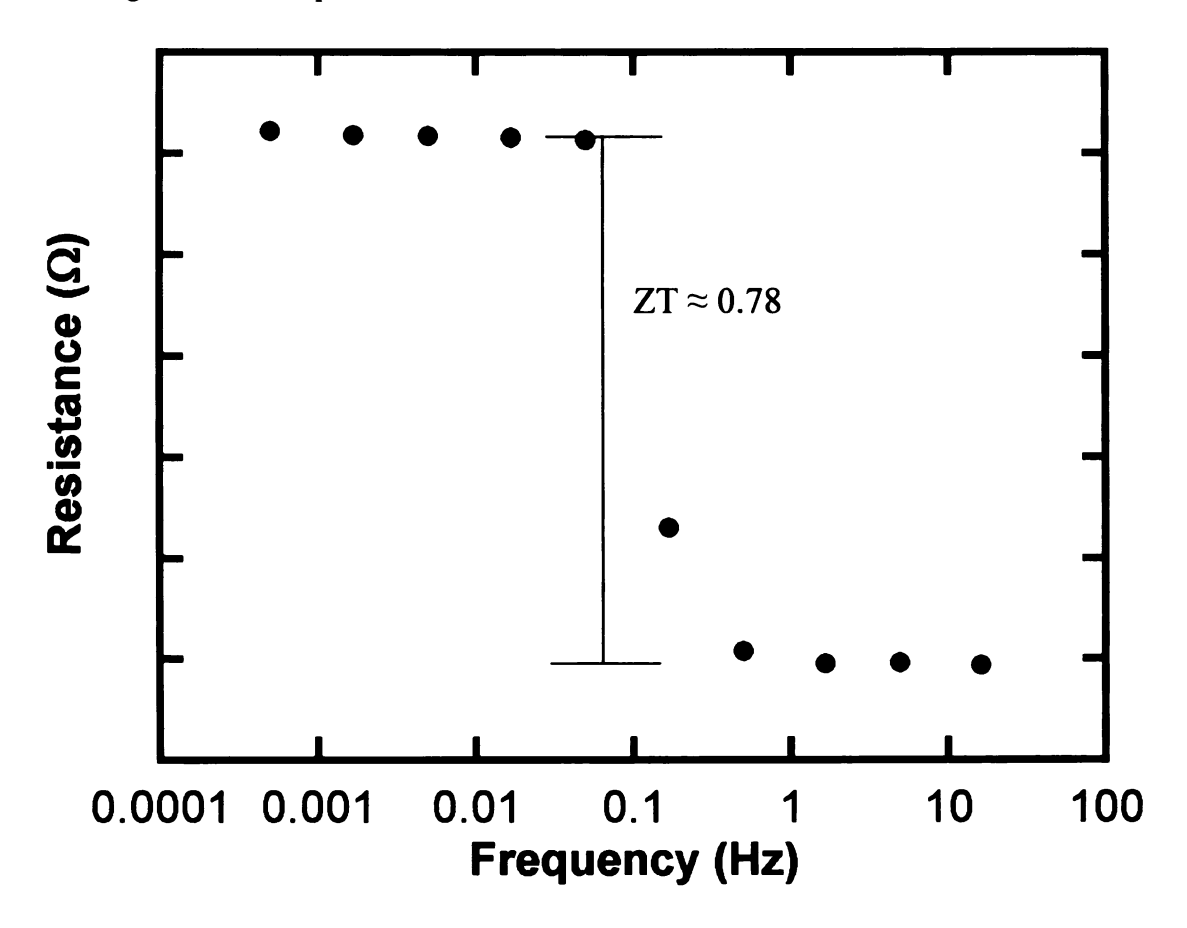


Figure 21. Example plot of resistance vs. frequency for a thermoelectric leg. Once measurements are completed, Equation (2.7) is used to calculate ZT.

$$ZT = \frac{R_{DC}}{R_{AC}} - 1 \tag{2.7}$$

Electrical conductivity is calculated using AC resistance, cross-sectional area, and length between the voltage probes according to Equation (2.8) below.

$$\sigma = \frac{1}{R_{AC}} \cdot \frac{s}{A} \tag{2.8}$$

CHAPTER 3

Results and Discussion

The following chapter outlines the results for the resistance, ZT, and electrical conductivity measurements. Unfortunately, after the experimental data had been collected, Smith discovered there were collinearities in the design. This is usually due either to small ranges of components, a large disparity between the proportions of the ranges, or a combination of both. Figure 22 shows the correlation of -0.9 between lead and tellurium. The negative correlation means that when the coefficient of lead is increased, the coefficient of tellurium is decreased. This means that the coefficients in the Scheffé polynomial are not correct. However, even though numerical values on the response surface plots cannot be trusted, the general trends predicted by the software are still useful. The collinearity is a property of the mixture design and applies to all of the resistance, ZT, and electrical conductivity response surfaces below.

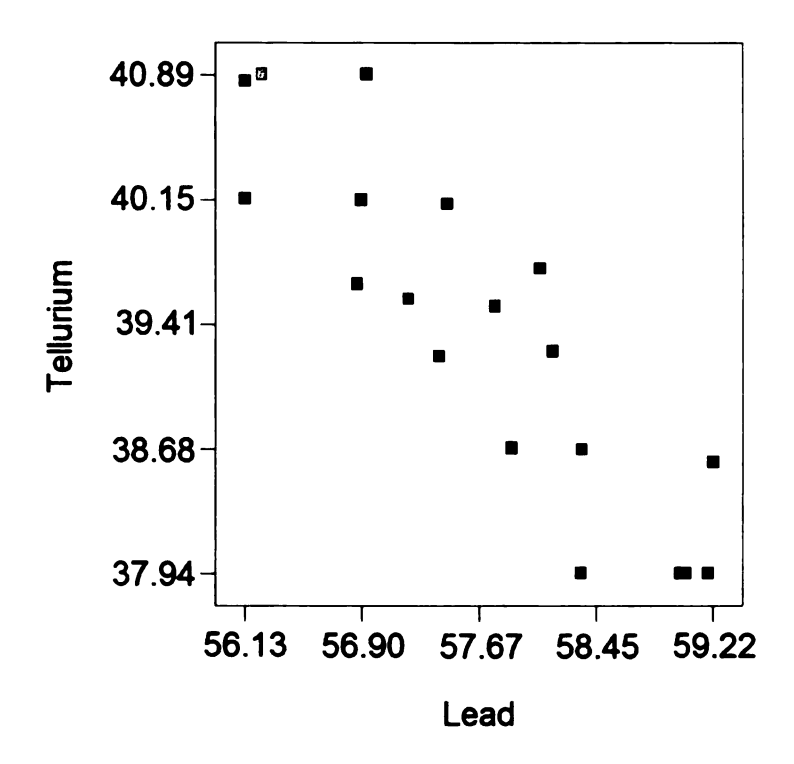


Figure 22. Correlation plot between tellurium and lead.

3.1 Resistance

Resistance data for each ingot is plotted below in Figure 23. In order to eliminate heteroscedasticity of the residuals, an inverse square root transformation was used.

Transformations are used to create homogeneity of variance and normality, and the inverse square root transformation was applied upon the recommendation of the Design-Expert® program. Heteroscedasticity of the residuals, or the undesirable cone shape, can be seen in Figure 24 below. Figure 25 shows the desired random scatter of the residuals after the transformation has been applied. Design point 14 was ignored for the statistical analysis. Figures 26 and 27 demonstrate these two changes. Figure 26 displays the predicted vs. actual plot for the resistance without any transformation or ignoring any data points. Figure 27 contains the predicted vs. actual plot after both changes have been applied.

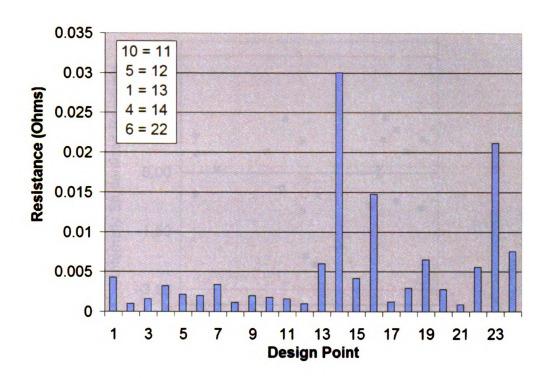


Figure 23. Resistance data plotted by design point.

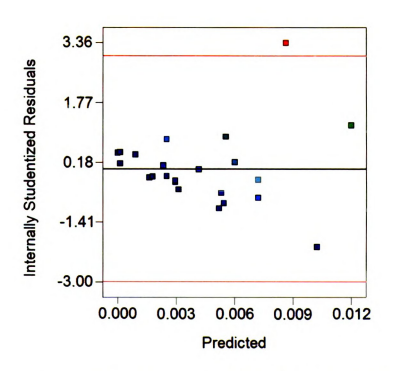


Figure 24. Internally studentized residuals vs. predicted resistance without inverse square root transformation.

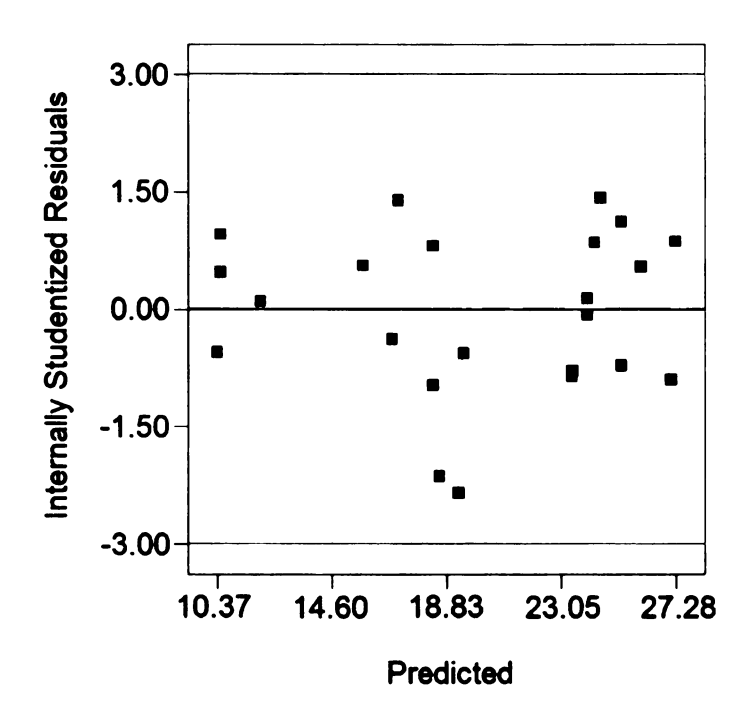


Figure 25. Internally studentized residuals vs. predicted resistance with inverse square root transformation.

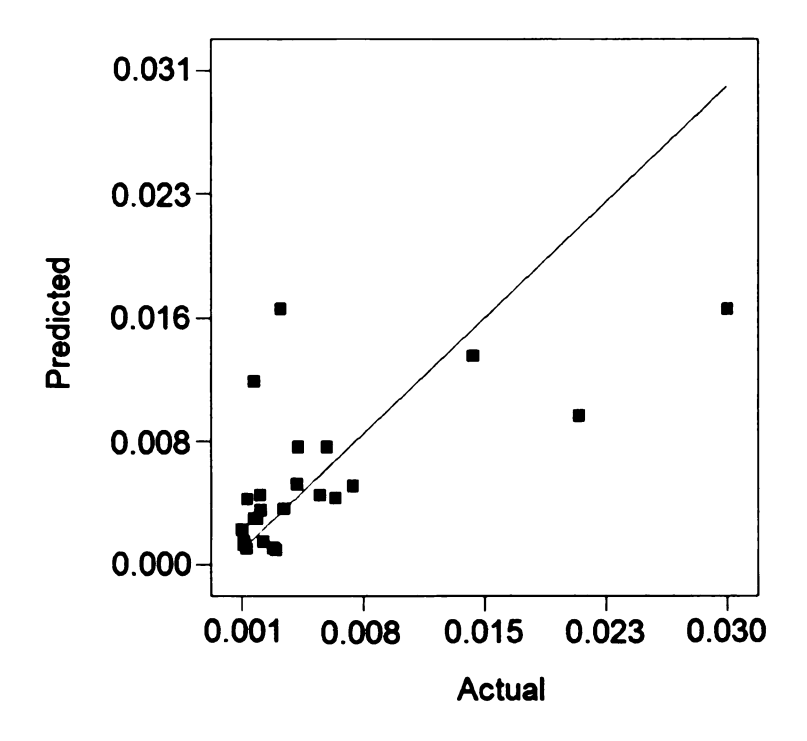


Figure 26. Predicted vs. Actual plot for resistance without transformation or ignored points.

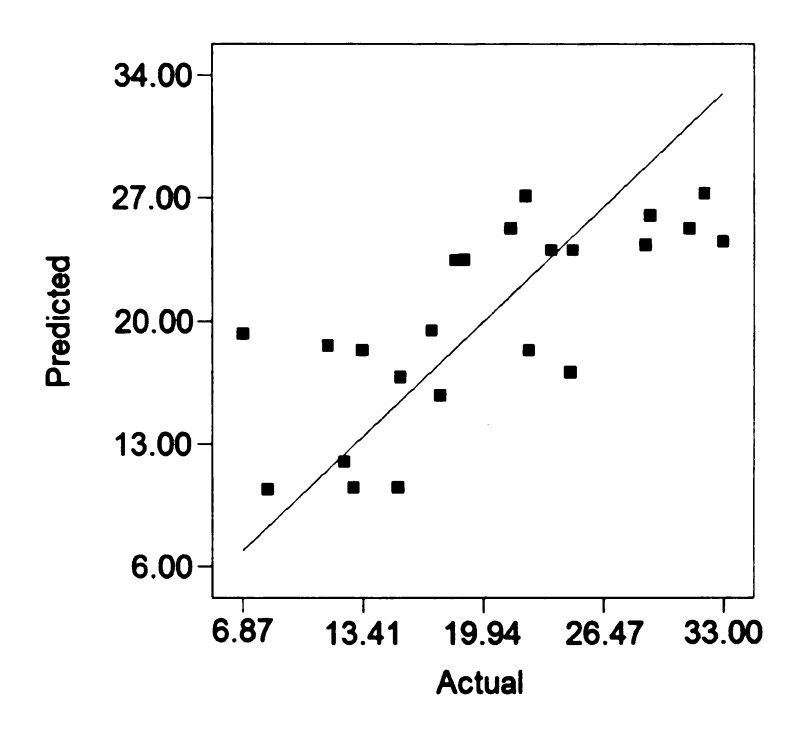


Figure 27. Predicted vs. Actual plot for resistance with point 14 ignored and the inverse square root transformation applied.

Table 4. ANOVA for quadratic model of transformed resistance response.

Source	Sum of Squares	DF	Mean Square	F-Value	p-value Prob > F
Model	673.39	9	74.82	1.64	0.2012
Linear Mixture	181.42	3	60.47	1.33	0.3076
AB	36.39	1	36.39	0.80	0.3875
AC	2.46	1	2.46	0.054	0.8198
AD	52.73	1	52.73	1.16	0.3014
BC	12.78	1	12.78	0.28	0.6051
BD	146.44	1	146.44	3.22	0.0962
CD	1.92	1	1.92	0.042	0.8404
Residual	591.76	13	45.52		
Lack of Fit	499.82	9	55.54	2.42	0.2052
Pure Error	91.94	4	22.98		
Cor Total	1265.15	22			

Table 5. R² values and adequate precision for the transformed resistance response fit.

R ²	R ² _{adj.}	R ² _{pred.}	Adeq. Precision
0.53	0.21	-0.82	3.80

The R² values are low, but this may be caused by the collinearities in the design.

The adequate precision, a signal-to-noise ratio, should be at a minimum of 4 for a reasonable fit. Due to the large number of imperfections in the material, it is not surprising the adequate precision values were low for all properties tested.

The response surface plots for resistance are shown below. The transformation has been applied, but plots are shown in the original scale. Three slices have been taken from the three-dimensional design space along the tellurium axis, where tellurium is equal to 37.945 g, 39.42 g, and 40.894 g. Note that the pink dots represent design points.

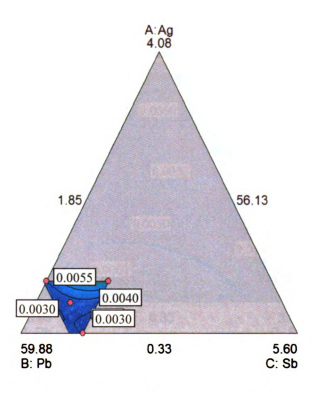


Figure 28. Contour plot of resistance at tellurium equal to 37.945 grams.

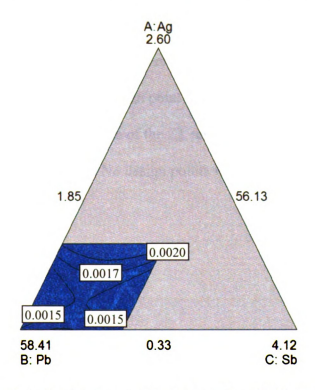


Figure 29. Contour plot of resistance at tellurium equal to 39.42 grams.

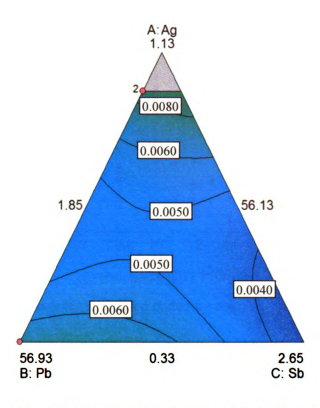


Figure 30. Contour plot of resistance at tellurium equal to 40.894 grams.

3.2 ZT

The scatter plot containing the ZT data is below. Points are color-coded by coin.

The ZT values for the statistical analysis were obtained by averaging the measured values for each leg to obtain one value per design point for entry into the Design-Expert*

software. A natural log transformation of the ZT response was modeled due to the heteroscedasticity of the residuals. No design points were removed for this analysis.

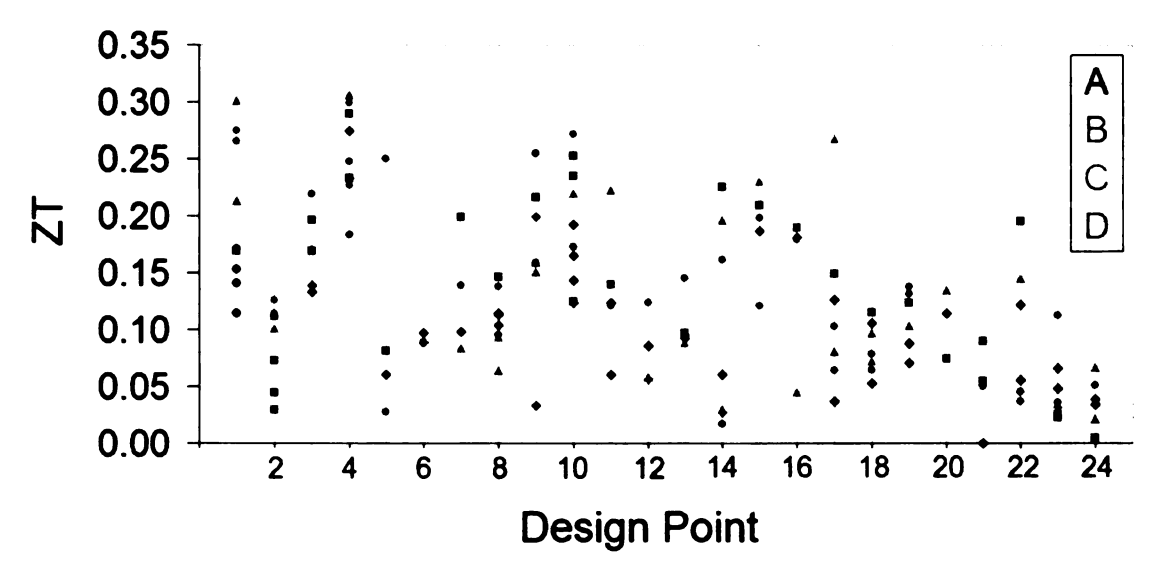


Figure 31. ZT data for each leg measured coded by coin.

The ANOVA for the quadratic Scheffé fit of ln(ZT) is in Table 6. Some may argue that a linear fit is more reasonable, but the extreme collinearity of the data causes exaggerated standard errors of the component estimates, especially those of terms consisting of silver and antimony. As a result, all model terms were included in order to avoid Type II error, or the error in concluding that a coefficient estimate is insignificant when the estimate is significant. As a result values in the ANOVA are not accurate; the tables below have been included for completeness.

Table 6. ANOVA for quadratic model of ln(ZT) response.

Source	Sum of Squares	DF	Mean Square	F-Value	p-value Prob > F
Model	1.88	9	0.21	1.10	0.4196
Linear Mixture	1.05	3	0.35	1.85	0.1844
AB	0.077	1	0.077	0.41	0.5344
AC	0.11	1	0.11	0.58	0.4588
AD	0.034	1	0.034	0.18	0.6798
BC	7.167E-004	1	7.167E-004	3.778E-003	0.9519
BD	0.069	1	0.069	0.37	0.5549
CD	2.450E-004	1	2.450E-004	1.291E-003	0.9718
Residual	2.66	14	0.19		
Lack of Fit	1.91	9	0.21	1.42	0.3645
Pure Error	0.75	5	0.15		
Corrected Total	4.54	23			

Table 7. R^2 values and adequate precision for ln(ZT) response fit.

R ²	R ² adj.	R ² _{pred.}	Adeq. Precision
0.41	0.04	-1.10	4.57

The contour plots for ZT are shown below. Responses are shown in the original scale, though the transformation has been applied.

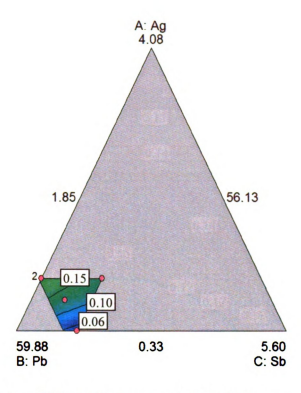


Figure 32. Contour plot of ZT at tellurium equal to 37.945 grams.

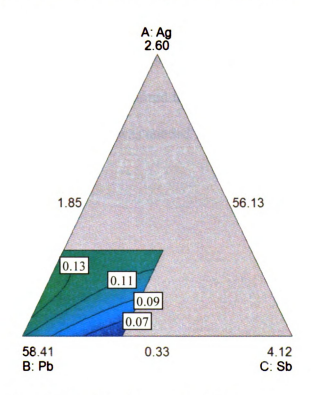


Figure 33. Contour plot of ZT at tellurium equal to 39.42 grams.

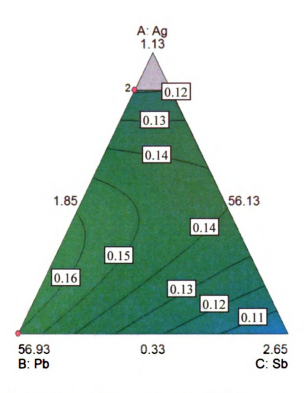


Figure 34. Contour plot of ZT at tellurium equal to 40.894 grams.

3.3 Electrical Conductivity

All electrical conductivity data points were averaged for each ingot. Due to the large difference in scale, point 12 was ignored for the statistical analysis of the electrical conductivity data. No transformation was needed for this response.

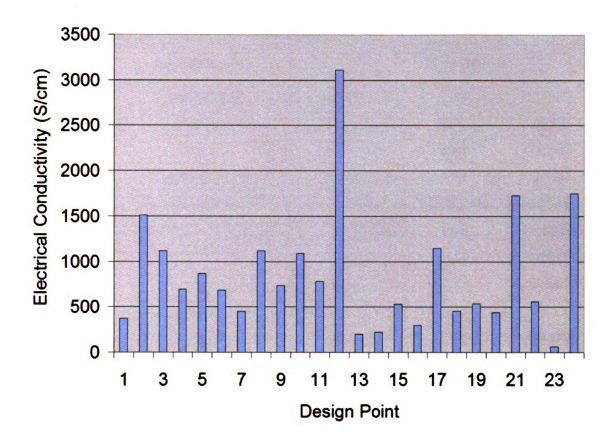


Figure 35. Electrical conductivity data plotted by design point.

The ANOVA and R^2 tables are provided below. Once again, inflated standard errors have led to insignificant p-values where significant p-values may exist.

Table 8. ANOVA for quadratic model of electrical conductivity data.

Source	Sum of Squares	DF	Mean Square	F-Value	p-value Prob > F	
Model	3.470E+006	9	3.856E+005	3.46	0.0211	
Linear Mixture	2.328E+006	3	7.758E+005	6.97	0.0049	
AB	2261.67	1	2261.67	0.020	0.8888	
AC	1.858E+005	1	1.858E+005	1.67	0.2189	
AD	1058.54	1	1058.54	9.511E-003	0.9238	
BC	1.826E+005	1	1.826E+005	1.64	0.2226	
BD	4.937E+005	1	4.937E+005	4.44	0.0552	
CD	1.948E+005	1	1.948E+005	1.75	0.2087	
Residual	1.447E+006	13	1.113E+005			
Lack of Fit	1.264E+006	9	1.404E+005	3.07	0.1459	
Pure Error	1.829E+005	4	45716.96			
Corrected Total	4.917E+006	22				

Table 9. R² values and adequate precision for electrical conductivity response.

R ²	R^2_{adj}	R ² _{pred}	Adeq. Precision
0.706	0.502	-0.02	7.39

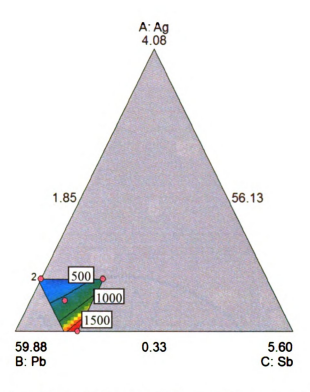


Figure 36. Contour plot of electrical conductivity at tellurium equal to 37.945 grams.

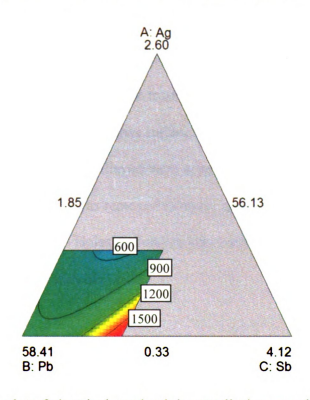


Figure 37. Contour plot of electrical conductivity at tellurium equal to 39.42 grams.

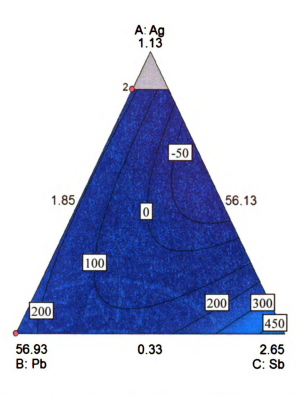


Figure 38. Contour plot of electrical conductivity at tellurium equal to 40.894 grams.

For comparison, Figure 39 shows the electrical conductivity response surface for tellurium equal to 40.894 grams when point 12 is included in the analysis. Though the predicted values on the contours cannot be trusted, it is interesting to see how one aberrant data point can affect the response surface. It is usually recommended that data points not be removed unless it is believed there is something wrong with the sample or measurement. Design point 12 was removed from the above analysis due to the known material properties of the legs. Holes and cracks were visible on many of the legs, suggesting that microcracks may also exist.

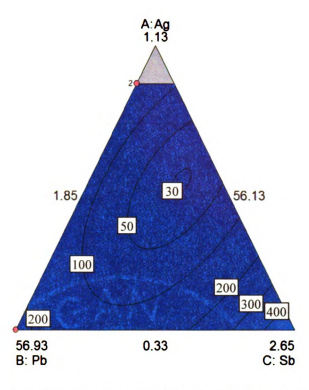


Figure 39. Contour plot of electrical conductivity at tellurium equal to 40.894 grams where all points were included in the analysis.

CHAPTER 4

Conclusions

Resistance, ZT, and electrical conductivity data have been analyzed for 24 cast ingots. The goal of the mixture experiment was to find a material with minimum electrical resistance, maximum ZT, and maximum electrical conductivity. Of these, maximum ZT is the most important. Unfortunately, poor material properties and collinearities have led to high variability and error. However, response surface plots can be used to determine general trends for future work. Figures 40 through 42 contain three-dimensional views of the fitted response surfaces for each property at different areas of interest.

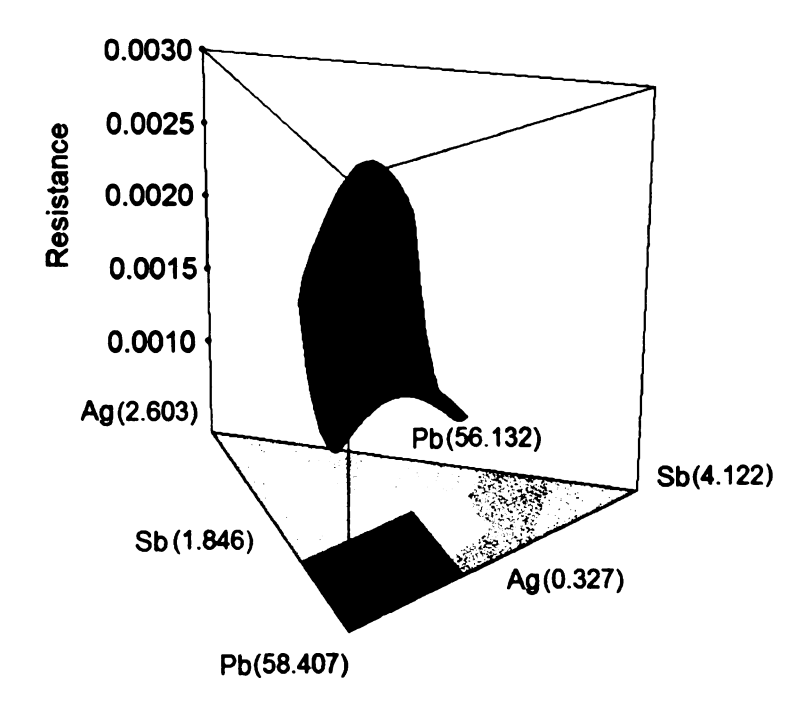


Figure 40. Three-dimensional view of resistance response surface at tellurium equal to 39.42 grams.

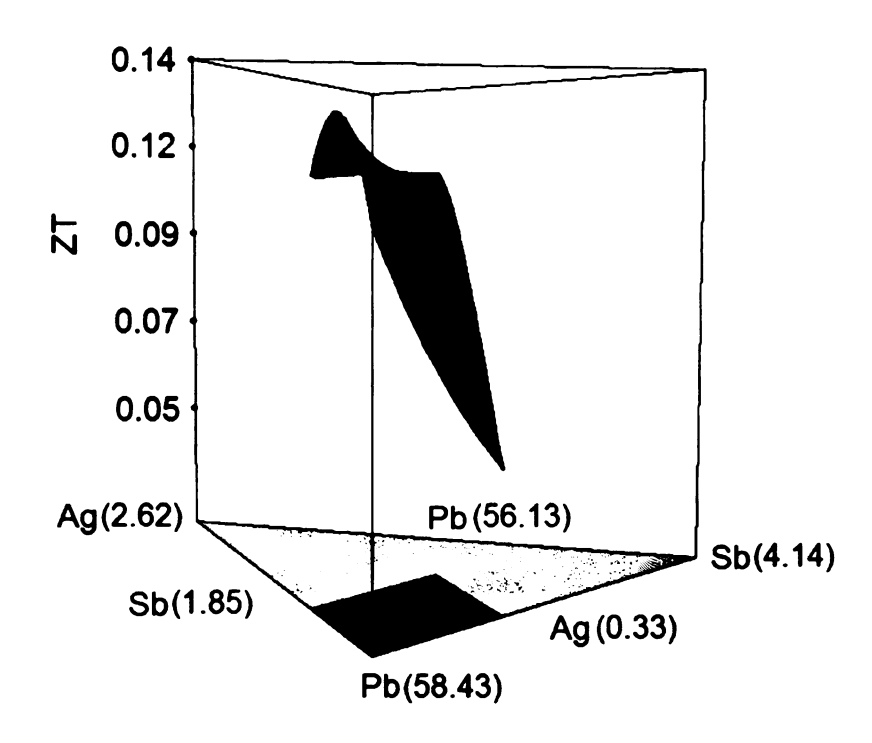


Figure 41. Three-dimensional view of ZT response surface at tellurium equal to 39.42 grams.

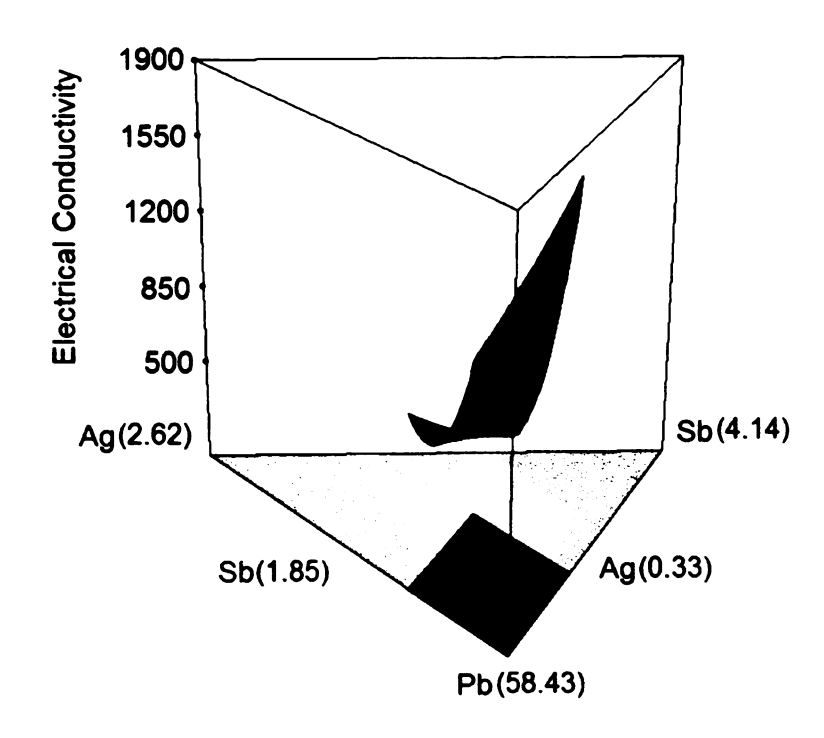


Figure 42. Three-dimensional view of electrical conductivity response surface at tellurium equal to 39.42 grams.

Table 10 summarizes the suggested levels of each component in order to optimize each property. There is agreement between all responses for components in lead and tellurium. However, an inverse relationship exists in silver between ZT and the other two responses, and in antimony between ZT and conductivity.

Table 10. Optimized component levels for tested properties.

	Ag	Pb	Sb	Te
Resistance	Low	High	Variable	Low
ZT	Max	Max	Min	Min
Electrical Conductivity	Min	High	Max	Low

CHAPTER 5

Recommendations

- One of the largest areas of needed improvement is in the reduction of
 variability at every step of the processes outlined above. The first step is to
 ensure the purity of the raw components as well as the accuracy of
 measurement of these components.
- 2. One issue that could be addressed in future research is the chemical makeup of the mixtures after undergoing the heating and cooling process. Members of the Michigan State thermoelectrics group have noticed traces of elements on the sides of the quartz tubes in which the ingots were cast, suggesting that the chemical composition prescribed was not the one tested. Methods of assessing the composition of finished ingots could prove statistically useful.
- I recommend that future mixture experiments be completed using ingots and legs that have better material properties than those used for the above experiment, since many imperfections were visible in the material. This may be accomplished by hot pressing the current materials or by using other types of thermoelectric material.
- 4. In order to reduce collinearity, the experimental design range sizes should be proportional and larger. If this cannot be accommodated, a standard response surface design should be used.

Appendices

Appendix A Additional Plot

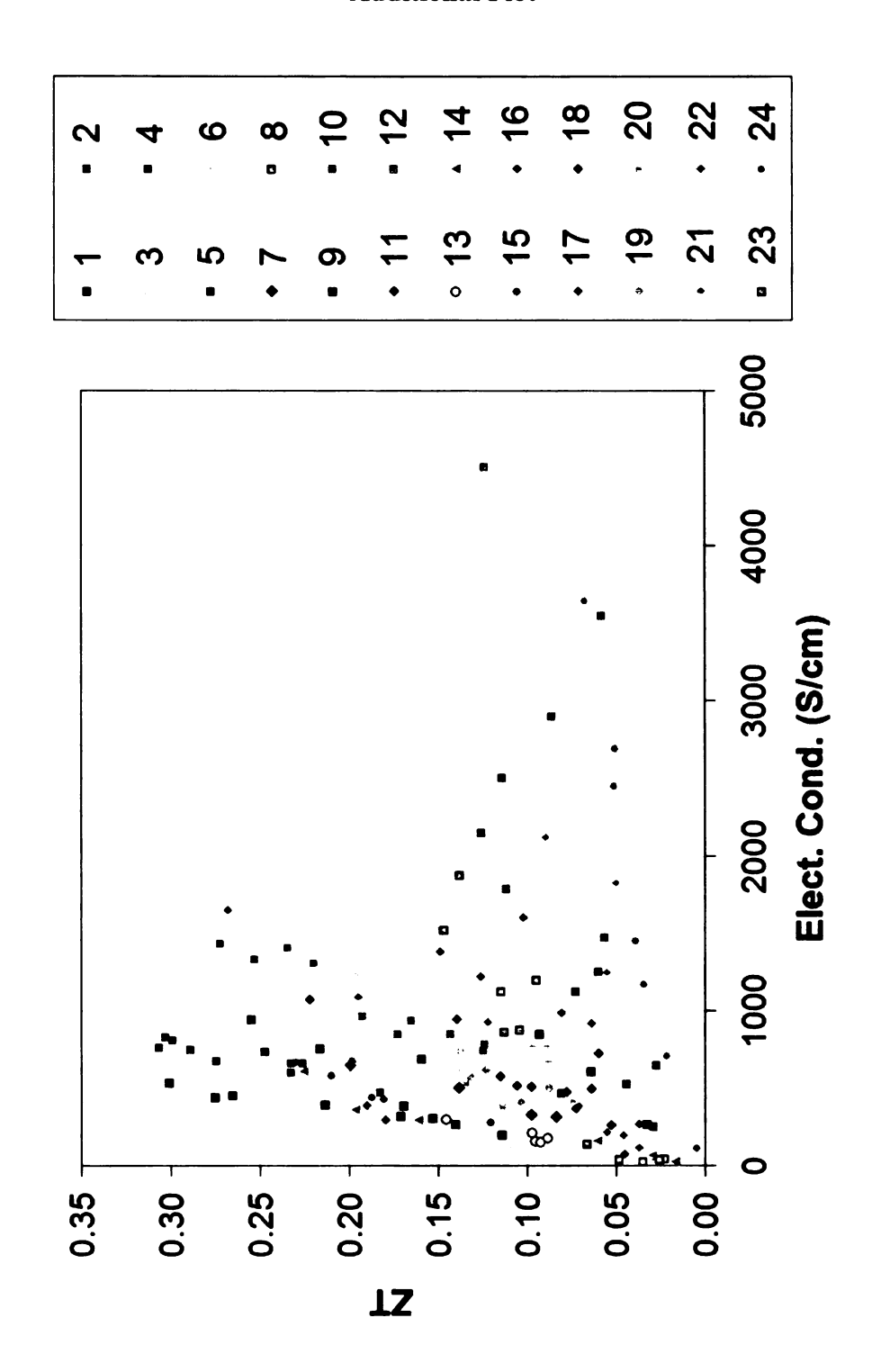


Figure 43. ZT vs. Electrical Conductivity for all design points.

Appendix B

ZT and Electrical Conductivity Data

Design Point	Coin	Leg	ZT	Average ZT	Electrical Conductivity	Average Electrical Conductivity
1	Α	1	0.114		198.900	
1	Α	4	0.140		269.838	
1	Α	5	0.153		309.600	
1	Α	6	0.171		321.228	
1	В	4	0.169		386.280	
1	С	4	0.214		397.764	
1	С	5	0.300		537.030	7.1
1	D	1	0.275		444.600	
1	D	6	0.265	0.200	456.552	369.088
2	В	1	0.111		1790.658	
2	В	2	0.029		256.284	
2	В	4	0.044		532.467	
2	В	6	0.073		1127.700	
2	С	1	0.101		2225.970	TANKS OF THE
2	D	1	0.126		2151.900	
2	D	3	0.114	0.085	2508.930	1513.416
3	Α	5	0.139		625.860	
3	Α	7	0.133		548.208	
3	В	2	0.169		773.046	
3	В	6	0.196	Marine Co.	1240.290	
3	D	4	0.219		2064.600	
3	D	5	0.170	0.171	1464.210	1119.369
4	Α	1	0.274		679.050	
4	Α	2	0.233		601.785	
4	В	1	0.289		749.943	
4	В	6	0.233		664.686	
4	С	1	0.306		763.758	
4	D	1	0.226	I QUELLE STATE	662.913	
4	D	2	0.30		828.24	
4	D	3	0.18		477.48	
4	D	4	0.25		736.56	37 18 18 18 18
4	D	5	0.30	0.26	813.67	697.809
5	Α	1	0.06		1254.33	
5	В	1-7	0.08		470.54	111111
5	D	4	0.03		650.21	A 1 1 1 1 1 1 1 1 1 1 1 1 1 1 1 1 1 1 1
5	D	4	0.25	0.10	1098.72	868.451

Figure 44. Data collected using ZT Machine (part 1).

Design Point	Coin	Leg	ZT	Average ZT	Electrical Conductivity	Average Electrical Conductivity
6	Α	3	0.098		770.580	
6	Α	4	0.088		771.930	
6	D	1	0.088		670.140	
6	D	3	0.087	0.090	515.160	681.953
7	Α	1-7	0.098		331.560	
7	В	5	0.199		647.640	
7	С	5	0.084		313.920	
7	D	1	0.139	0.130	503.010	449.033
8	Α	2	0.114		1124.862	
8	Α	4	0.104		874.872	
8	Α	6	0.113		864.036	
8	В	1	0.146		1521.900	
8	С	4	0.064		609.435	
8	С	7	0.093		853.875	
8	D	1	0.095		1201.680	
8	D	1-7	0.138	0.108	1873.710	1115.546
9	Α	4	0.033		267.039	
9	Α	6	0.199		570.060	
9	В	3	0.216		758.097	
9	С	6	0.151		645.120	
9	С	7	0.160		693.594	
9	D	2	0.158		1261.980	
9	D	6	0.255	0.167	943.560	734.207
10	Α	4	0.192		850.422	
10	Α	7	0.165		783.363	
10	Α	1-7	0.143		966.690	
10	Α	1-7	0.124		935.280	
10	В	1	0.253		1334.880	
10	В	2			747.090	
10	В	4	0.234		1388.225	
10	В	1-7	0.124		1408.950	
10	С	4	0.220		1305.347	
10	D	1-7	0.272		1433.502	
10	D	1-7	0.172	0.190	850.410	1091.287
11	Α	2	0.124		784.260	M26 7 3 7
11	Α	4	0.060		722.106	
11	В	7	0.140		942.570	
11	C	7	0.222		1075.590	
11	D	5	0.120	0.133	374.310	779.767

Figure 45. Data collected using ZT Machine (part 2).

Design Point	Coin	Leg	ZT	Average ZT	Electrical Conductivity	Average Electrical Conductivity
12	Α	3	0.086		2899.800	
12	Α	5	0.056		1477.080	
12	С	2	0.058		3554.010	
12	D	7	0.124	0.081	4511.430	3110.580
13	Α	2	0.095		163.350	
13	Α	7	0.093		155.790	
13	В	1	0.097		211.950	
13	С	1	0.088		178.110	
13	D	7	0.145	0.104	299.250	201.690
14	Α	3	0.028		37.471	
14	Α	4	0.060		163.670	
14	В	4	0.225		607.410	
14	С	1	0.197		362.070	
14	С	4	0.030		69.840	
14	D	1	0.017		27.360	
14	D	2	0.161	0.103	293.180	223.000
15	Α	1	0.187		441.540	
15	В	5	0.210	GARE	584.730	
15	С	1-7	0.230		672.840	
15	D	5	0.198		680.040	
15	D	7	0.121	0.189	279.450	531.720
16	Α	5	0.181		428.265	
16	В	3	0.190		391.842	
16	С	1-7	0.046		71.302	
16	D	2	0.180	0.149	296.280	296.922
17	Α	2	0.037		268.857	
17	Α	3	0.126		1219.860	
17	В	3	0.149		1379.520	
17	С	1	0.081		986.760	
17	С	4	0.268		1651.320	
17	D	1	0.102		1605.060	
17	D	6	0.064	0.118	919.530	1147.272
18	Α	6	0.053		260.558	
18	Α	7	0.106	or Leaves district	516.897	
18	В	4	0.115		575.496	705 ST 50 15
18	C	2	0.098		508.388	MANUFACTURE AND ADDRESS.
18	C	6	0.073	2	369.257	
18	D	4	0.064		495.540	
18	D	7	0.078	0.084	474.120	457.179

Figure 46. Data collected using ZT Machine (part 3).

Design Point	Coin	Leg	ZT	Average ZT	Electrical Conductivity	Average Electrical Conductivity
19	Α	1	0.071		380.070	100
19	Α	2	0.088		495.000	
19	В	7	0.123		615.879	Transfer in
19	С	5	0.103		405.945	
19	D	3	0.131		570.807	
19	D	7	0.138	0.109	739.206	534.485
20	Α	3	0.114		375.480	
20	В	5	0.074		418.140	STAN THE
20	С	3	0.134	0.108	524.880	439.500
21	В	6	0.090		2118.060	
21	В	7	0.055		1244.525	
21	D	7	0.050	0.065	1825.470	1729.352
22	Α	4	0.122		922.140	
22	Α	5	0.055		211.599	
22	В	4	0.195		1087.650	
22	С		0.145		823.410	
22	D	4	0.037		111.528	
22	D	5	0.046	0.100	195.030	558.560
23	Α	1	0.066		143.640	
23	Α	6	0.048		41.009	
23	В	3	0.023		44.204	
23	В	7	0.026		42.835	
23	С	2	0.035		29.238	
23	D	5	0.112		31.950	
23	D	5	0.036	0.049	88.740	60.231
24	Α	1	0.034		1169.910	
24	Α	1-7	0.039		1457.088	
24	В	4	0.004		116.370	
24	С	1	0.021		708.532	46.70633
24	С	6	0.067		3647.803	
24	D	4	0.051		2697.170	
24	D	5	0.051	0.038	2456.297	1750.453

Figure 47. Data collected using ZT Machine (part 4).

References

References

- 1. Agreda, C.L. and V.H. Agreda, Designing Mixture Experiments. *ChemTech*, 1989. 19(9): p. 3.
- 2. Cornell, J.A., *Experiments with Mixtures*. 2nd ed. Wiley Series in Probability and Mathematical Statistics. 1990, New York: Wiley-Interscience.
- 3. Cornell, J.A., A Comparison Between Two Ten-point Designs for Studying Three-component Mixture Systems. *Journal of Quality Technology*, 1986. **18**(1): p. 15.
- 4. Downey, A.D., Advancing Thermoelectrics Research with New Measurement Systems and Thermoelectric Modeling for AC Electrical Measurements. 2006, Michigan State University: East Lansing, Michigan.
- 5. Hsu, K.F., et al., Cubic AgPb_mSbTe_{2+m}: Bulk Thermoelectric Materials with High Figure of Merit. *Science*, 2004. **303**(5659): p. 4.
- 6. Humphry, T.E., et al., Reversible Thermoelectric Nanomaterials. *Physical Review Letters*, **94**(9): p. 4.
- 7. Ioffe, A.F., Semiconductor Thermoelements and Thermoelectric Cooling. Infosearch Limited, 1957, London.
- 8. Kosuga, A., et al., Thermoelectric Properties of Ag_{1-x}Pb₁₈SbTe₂₀ (x=0, 0.1, 0.3). Journal of Alloys and Compounds, 2005. **387**(1-2): p. 3.
- 9. Mason, R.L., R.F. Gunst, and J.L. Hess, Statistical Design and Analysis of Experiments: with Applications to Engineering and Science. 1989, New York: Wiley.
- 10. Rice, J.A., *Mathematical Statistics and Data Analysis*. 1988, Monterey, Calif.: Brooks/Cole Pub. Co.
- 11. Rowe, D.M., CRC Handbook of Thermoelectrics. 1995, Boca Raton, FL: CRC Press.
- 12. Scheffé, H., Experiments with Mixtures. *J. Royal Statistical Soc. B*, 1958. **20**(2): p.16
- 13. Schenck, H.V.N., *Theories of Engineering Experimentation*. 2d ed. 1968, New York,: McGraw-Hill.
- 14. Smith, Wendell F., Experimental Design for Formulation. ASA-SIAM Series on Statistics and Applied Probability, SIAM, Philadelphia, ASA, Alexandria, VA, 2005.

- 15. Smith, W.F., Data Set E-mail, K. Sarbo, Editor. 2006: East Lansing, Michigan.
- 16. Smith, W.F., *Mixture Experiment E-mail*, K. Sarbo, Editor. 2006: East Lansing, Michigan.
- 17. Smith, W.F., *Collinearity E-mail*, K. Sarbo, Editor. 2006: East Lansing, Michigan.
- 18. Smith, W.F., Data E-mail, K. Sarbo, Editor. 2006: East Lansing, Michigan.
- 19. Stat-Ease, *Design-Expert*. 2006, Stat-Ease, Inc.: Minneapolis.
- 20. Stat-Ease, Mixture Design for Optimal Formulations. 2006, Stat-Ease, Inc.: Minneapolis.
- 21. Tellurex. An Introduction to Thermoelectrics. 2001 [cited; Available from: http://www.tellurex.com/cthermo.html.
- 22. Wang, H., et al., High-performance Ag_{0.8}Pb_{18+x}SbTe₂₀ Thermoelectric Bulk Materials Fabricated by Mechanical Alloying and Spark Plasma Sintering. *Applied Physics Letters*, 2006. **88**(9): p. 3.

